Japanese Journal of Applied Physics

The Japan Society of Applied Physics

RAPID COMMUNICATIONS • OPEN ACCESS

Tunable plasmonic nanocavity with $Ge_2Sb_2Te_5$ film for directional launching of surface plasmons

OPEN ACCESS

Japanese Journal of Applied Physics **57**, 040307 (2018)

https://doi.org/10.7567/JJAP.57.040307

RAPID COMMUNICATION

Tunable plasmonic nanocavity with $Ge_2Sb_2Te_5$ film for directional launching of surface plasmons

Hee-Dong Jeong[1], Chi-Young Hwang[2], Hyuntai Kim[3], Muhan Choi[1], and Seung-Yeol Lee[1]*

[1]*School of Electronics Engineering, Kyungpook National University, Daegu 41566, Republic of Korea*
[2]*Reality Display Device Research Group, Electronics and Telecommunications Research Institute, Daejeon 34129, Republic of Korea*
[3]*Optoelectronics Research Centre, University of Southampton, Southampton SO17 1BJ, U.K.*

*E-mail: seungyeol@knu.ac.kr

Received December 1, 2017; accepted January 8, 2018; published online February 27, 2018

A tunable plasmonic nanocavity which consists of a metallic groove with submerged ultra-thin $Ge_2Sb_2Te_5$ film is proposed for controlling the on/off characteristics of directional surface plasmon polaritons (SPPs) launching. Different mechanisms of launching SPPs using two orthogonal incident polarizations are investigated to reveal the SPP generation characteristics from the proposed nanocavity. By choosing the appropriate position of $Ge_2Sb_2Te_5$ film, we report that the directional launching characteristics of SPPs can be controlled by changing the phase state of extremely small volume of $Ge_2Sb_2Te_5$ film, which shows up to 37 dB of extinction ratio changing characteristics. © 2018 The Japan Society of Applied Physics

Surface plasmon polaritons (SPPs) has been greatly contributed to the various fields of nanophotonics,[1)] since SPPs can be highly confined below the diffraction limit and strongly related to the aspect of electron dynamics on metal surfaces.[2)] Such properties of SPPs make possible to develop numerous integrated plasmonic devices such as plasmonic lens,[3)] negative refractive index waveguides,[4,5)] directional launchers,[6,7)] fiber sensors,[8)] and metasurfaces.[9–11)] Especially, fascinating research fields that focused on observing extraordinary nature of SPPs caused by strong light-matter interaction are demonstrated, such as spin–orbit interaction in plasmonic vortex lenses,[12)] photonic spin-Hall effects,[13)] and nonlinear effects[14)] because these phenomena are usually very weak in typical dielectric-based photonic structures. Therefore, plasmonic devices to which these phenomena are intuitively applied can provide an alternative route for overcoming the limitations of conventional optical device such as diffraction limits.

One of recent demands for improving these devices is giving a tunable functionality to them by using active materials. Various candidate materials are still competitive for active tuning of SPPs; such as graphenes,[15,16)] liquid crystals on silicon,[17)] VO_2,[18)] and chalcogenide phase change materials such as $Ge_2Sb_2Te_5$ (GST), etc.[19–21)] Among of them, active plasmonic devices using the phase change characteristics of GST are tentatively reported within recent years since GST has unique characteristics such as a very large permittivity change in wideband spectrum from visible to mid-infrared, non-volatile, reconfigurable, and high compatibility with conventional semiconductors.[22)] Hence, the recent publications shows that GST can be highly applicable to various nanophotonic applications such as all-optically driven memory, active metasurfaces, tunable perfect absorber, and holographic display panels.[19–25)]

In nanoslit excitation problem, it has been shown that the electron dynamics near the nanoslit caused by incident electric fields or magnetic induction currents can strongly affect to the launching direction and phase of SPPs.[26)] Spatially changing phase profile of an incident magnetic field perpendicular to nanoslit (transverse magnetic, TM) polarization with an obliquely incident wave can provide symmetric parity of excited SPPs, whereas anti-symmetric parity of excited SPPs is formed by perpendicular-to-slit electric field (transverse electric, TE) polarization. As a result, a unidirectional launching of SPPs was demonstrated which can be controlled by incident polarization by the interference of two different type of SPP excitation.[26)] However, to the best of our knowledge, there was almost no attempt to apply active material to selectively tune the spin-assisted directional launching characteristics because it was not easy to simultaneously optimize the structure for both states of phase change material.

In this paper, we proposed a tunable plasmonic nanocavity which has submerged half-transparent thin GST film laid on subwavelength-size metallic groove. Numerical simulations based on rigorous coupled wave analysis (RCWA)[27)] show that the GST layer can be used for utilizing the tunable characteristics of spin-assisted directional launching of SPPs. The key idea of our tunable nanocavity for directional launching of SPPs is based on the following mechanism. At first, we found the most effective position of inserted GST, which means that the change of the TE/TM SPP coupling ratio is maximized before and after the crystallization of GST. Then, the ratio of TE/TM SPP coupling coefficients are designed to the nearly identical value for the amorphous GST insertion case, which is related to the unidirectional-on state of the proposed structure. Because the structure is designed to have the greatest change of TE/TM SPP coupling ratio, such unidirectional-on state can be turn-off when the inserted GST layer is crystallized.

A schematic of the proposed plasmonic nanocavity is shown in Fig. 1(a). An obliquely incident light which has a plane of incidence of y-z plane illuminates the proposed structure. Throughout the paper, the nanocavity is composed of three layers—upper-dielectric, GST, and lower-dielectric—of which the thicknesses are defined to d_1 d_{GST}, and d_2, as depicted in Fig. 1(b). Throughout the manuscript, the width of nanocavity (w) and free space incident wavelength (λ) are fixed to $w = 150$ nm and $\lambda = 633$ nm. The width of the nanocavity is sufficiently narrow so that only the fundamental plasmonic mode can propagate inside the MIM region.[28)] Relative permittivity of dielectric layer is assumed to non-dispersive ($\varepsilon_d = 2.25$), whereas that of gold (ε_{Au}), and GST

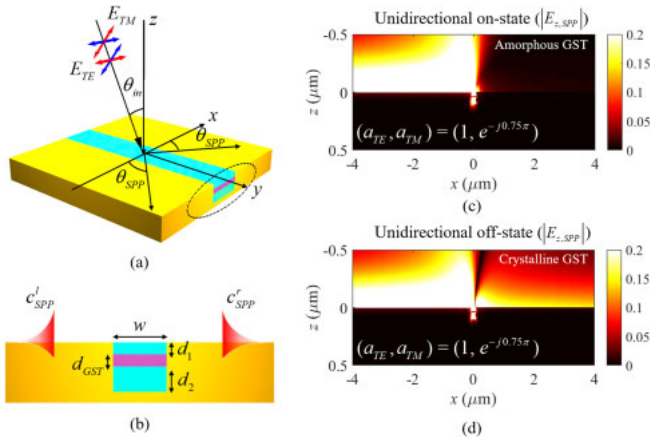

Fig. 1. (Color online) (a) Schematic of the proposed nanocavity for tunable directional launching of SPPs. Red and blue arrows indicate the directions of electric and magnetic field for each polarization, respectively. (b) Cross-sectional view of the proposed nanocavity with definitions of geometric parameters. (c) Excited SPP distributions of the designed structure when submerged thin GST is in amorphous state (On-state) or (d) in crystalline state (Off-state). The parameters θ_{in}, d_1, d_{GST}, d_2, and w are set to 40°, 30, 10, 70, and 150 nm, respectively.

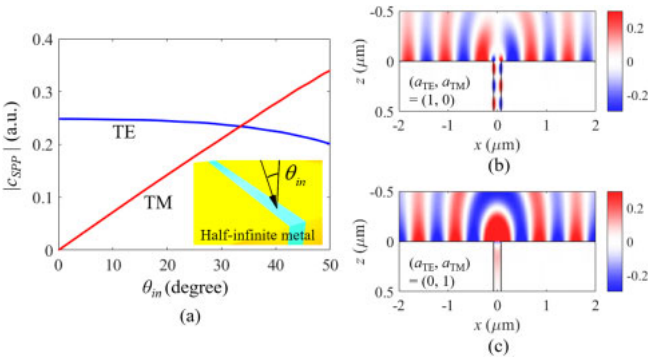

Fig. 2. (Color online) (a) SPP excitation characteristics for TE and TM polarization incidences with oblique incident angle along y-z plane, half-infinite thickness of metal substrate. Excited SPP distributions for (b) TE and (c) TM incident polarizations, which shows anti-symmetric parity for TE incidence and symmetric parity for TM incidence, respectively.

(ε_{GST}) are determined by referring the experimental results conducted by previous researches.[21,29] At designing wavelength (633 nm), the relative permittivity of Au is given as $\varepsilon_{Au} = -10.6 + 1.27i$, and the refractive indexes of GST for amorphous and crystalline states are $n_{GST,am} = \sqrt{\varepsilon_{GST,am}} = 4.05 + 2.14i$, and $n_{GST,cry} = \sqrt{\varepsilon_{GST,cry}} = 3.39 + 4.26i$, respectively. It is noteworthy that the huge change of imaginary part of refractive index is observed during the crystallization of the GST, which is the main mechanism for tunable SPP excitation. It is known that both polarizations can excite SPP when $\theta_{inc} \neq 0$.[26] Regardless of its polarization states, momentum matching condition along y-direction can determine the propagation angle of SPP (θ_{SPP}) as follows:

$$\theta_{SPP} = \sin^{-1}\left(\frac{\sin\theta_{in}}{n_{SPP}}\right), \quad (1)$$

where $n_{SPP} = \mathrm{Re}\left[\sqrt{(\varepsilon_{air}\varepsilon_{Au})/(\varepsilon_{air} + \varepsilon_{Au})}\right]$ is an effective refractive index of SPP mode and ε_{air}, ε_{Au} indicate relative permittivity of air and gold, respectively. Interference of SPP excited by TE and TM incidence can lead to the unidirectional launching of SPP at the certain Jone's vector conditions of $\mathbf{J} = (a_{TE}, a_{TM}) = (c^{l}_{SPP,TM}, \pm c^{l}_{SPP,TE})$ due to the opposite parity of excited SPPs.[26] Here, $c^{l}_{SPP,TE}$ and $c^{l}_{SPP,TM}$ indicates the coupling coefficients of SPPs through the left-side excited by TE or TM polarization, and plus or minus sign indicates the left- or right-side unidirectional launching condition, respectively. In addition, we add a GST film as a function of active layer to tune the directional launching characteristics. Figures 1(c) and 1(d) show the E_z field amplitude of excited SPP with the optimized parameters designed for tunable unidirectional launching. Here, the on-/off-switching of directional launching characteristics can be done by only changing the amorphous/crystalline state of 10 nm thickness GST layer. We first consider the case of half-infinite metal substrate as shown in the inset of Fig. 2(a). As depicted in Fig. 2(a), it is shown that SPP excitation caused by TE polarization has the largest amount for normal incidence and slightly decrease when incident angle increases. On the other hand, TM polarized incidence does not make any SPPs for normal incidence but the amount of excited SPP gradually increases when incident angle increases. It is shown that the amount of SPP excited by TM wave overtakes that by TE wave at 34°, but the SPP excited by TM wave may reduce due to the insertion of thin GST-layer (details are discussed below). Considering such effect, incident angle for proposed structure is designed to 40°, which is comparably larger than the crossing point. The electric field distributions for TE and TM incident fields are shown in Figs. 2(b) and 2(c). The SPP excited by TE polarization has anti-symmetric parity on the top surface of metal film, whereas that by TM polarization has symmetric excitation parity. Hence, the superposition of two different incidences may lead to directional launching of SPPs, the detail procedure of the electron dynamics of given circumstance can be found in our previous works.[26]

Figure 3(a) shows the schematic for explaining the effect of thin GST insertion for TE polarization. Since the fundamental plasmonic mode can propagate inside the cavity, Fabry–Perot resonance (FPR) in the nanocavity is strongly observed. In order to maximize the excitation characteristics of SPP by simply tuning the crystallization characteristics of inserted GST, we have to carefully design the position and thickness of GST layer.

When the thickness of the GST film is too thin, the effect of phase transition may be too small. On the other hand, thicker GST film makes higher reflection at the first dielectric-GST interface and it also reduce the effect of FP resonance inside the cavity. Therefore, there is an appropriate thickness value in GST thickness which is neither too thin nor too thick. This value was evaluated by both experimentally and theoretically in our previous works, which is about 7–10 nm scale.[21]

Now we would like to consider the efficient position of inserted GST layer. One can easily suppose that inserting GST layer at the appropriate position where electric field is maximized can be the best choice for increasing modulation efficiency. The right positions for GST inserting are marked by purple dotted squares, which are the antinode of standing wave formed by FPR of the nanocavity that satisfy the following conditions,

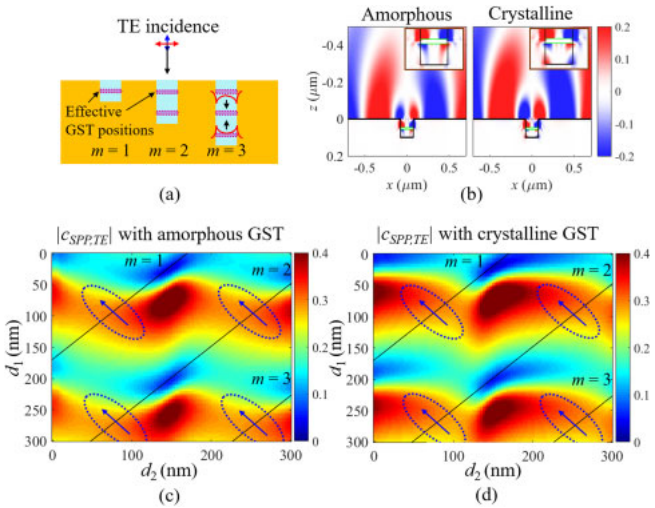

Fig. 3. (Color online) (a) Appropriate position of thin GST for efficient change of TE incident SPP coupling coefficient. (Red and blue arrows represent the direction of the electric and magnetic field, respectively.) (b) Field distribution at $m = 1$ condition ($d_1 = 45$ nm, $d_2 = 45$ nm) for amorphous and crystalline GST insertion. Insets show the expanded field image inside the cavity. Characteristic of TE incident SPP coupling coefficients varying with two parameters, d_1 and d_2; for (c) amorphous GST and (d) crystalline GST cases, respectively.

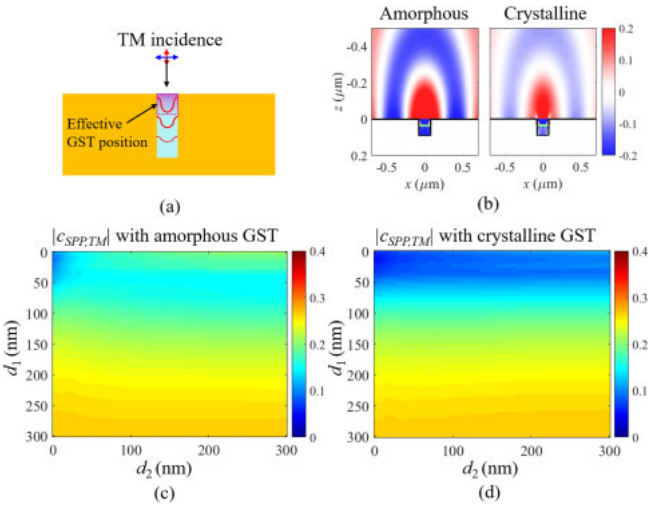

Fig. 4. (Color online) (a) Appropriate position of thin GST for efficient change of TM incident SPP coupling coefficient. (b) Field distribution at the appropriate condition ($d_1 = 30$ nm, $d_2 = 70$ nm) for amorphous and crystalline GST insertion. Characteristic of TM incident SPP coupling coefficients varying with two parameters, d_1 and d_2; for (c) amorphous GST and (d) crystalline GST cases, respectively.

$$d_1 = (2l-1)\frac{\lambda_{z,\mathrm{MIM}}}{4} \text{ and } d_1 + d_2 = m\frac{\lambda_{z,\mathrm{MIM}}}{2}, \quad \begin{cases} m = 1, 2, 3, \ldots \\ l = 1, 2, \ldots, m \end{cases}, \tag{2}$$

where $\lambda_{z,\mathrm{MIM}}$ is determined by the z-directional wavevector of the MIM mode inside the cavity,

$$\lambda_{z,\mathrm{MIM}} = \frac{2\pi}{k_{z,\mathrm{MIM}}} = \frac{2\pi}{k_0\sqrt{n_{\mathrm{MIM}}^2 - \sin^2\theta_{\mathrm{in}}}}, \tag{3}$$

where n_{MIM} is the effective refractive index of fundamental MIM plasmonic mode, determined by geometric parameters of nanocavity.

Figure 3(b) shows the $E_{z,\mathrm{SPP}}$ field distributions of the proposed nanocavity when the inserted GST is either amorphous or crystalline state, respectively. As discussed, the phase profile inside the cavity is changed after crystallization of GST, which is clearly observed in the insets of Fig. 3(b). By comparing Figs. 3(c) and 3(d), the aspect of excited SPP for TE polarization incidence can be observed when the phase of the inserted GST layer is changed from amorphous to crystalline. When the slit width is fixed to $w = 150$ nm, the effective index and the wavelength of the MIM mode is calculated as $n_{\mathrm{MIM}} = 1.89$ and $\lambda_{z,\mathrm{MIM}} = 358$ nm by using the analytic solution of MIM plasmonic mode with the incident angle condition of $\theta_{\mathrm{in}} = 40°$. The black solid lines shown in Figs. 3(c) and 3(d) indicate the appropriate total thickness of the nanocavity that satisfy the latter condition of Eq. (2), and the regions circled by blue dotted line show the interested region where the effect of GST phase transition is dramatically observed. Similar to previously-reported work,[21] the shift of resonance occurs toward the upper-left direction of Figs. 3(c) and 3(d), which indicates the effective optical length of cavity can be reduced by the GST crystallization, because the phase lagging or leading characteristics after passing through the thin-GST layer can be tuned by the change of refractive index of GST layer.[21]

From now, we would like to discuss the SPP excitation characteristics for TM wave incidence of the proposed structure. Since there is no propagating mode inside the cavity, penetrated electric field of TM incidence will slowly decay inside the cavity as depicted in Fig. 4(a). In this case, permittivity change of GST layer can affect to the total amount of infiltrated incident field into the nanocavity region. This phenomenon can only occur when GST layer is located extremely close to the entrance of nanocavity. Figure 4(b) compares the $E_{z,\mathrm{SPP}}$ field distributions before and after the GST phase transition. In this case, the amount of excited SPP can significantly decreased when GST layer is crystallized. This can be understood because crystalline GST has more metal-like permittivity [$\mathrm{Re}(\varepsilon_{\mathrm{GST}}) < 0$] than that of amorphous GST at the designed wavelength, change from amorphous phase to crystallized state will significantly reduce the penetrated electric field inside the cavity. Similar to TE case, the aspect of excited SPP for TM polarization incidence can be observed by comparing Figs. 4(c) and 4(d) when the phase of the inserted GST layer is changed from amorphous to crystalline. One can clearly found that coupling coefficient for TM incidence only varies when GST film is located near to the upper edge of the cavity. In other words, parameter d_1 should be sufficiently small (less than 50 nm) to affect the coupling coefficient for TM incidence.

By investigating the SPP excitation characteristics of the proposed geometry, we can deduct the appropriate length of cavity and the position of inserted GST layer. Thinner d_1 value can increase the effect of GST phase transition for TM polarization, and positions where the antinodes of FPR locate is the most effective GST position for TE incidence. Since coupling coefficients for TE incidence increase and that for TM incidence decrease when inserted GST is crystallized, TE/TM SPP coupling ratio will significantly increases where the abovementioned two conditions are overlapped. Figure 5 shows the figure of merit (FOM) parameter of the proposed structure which is defined as

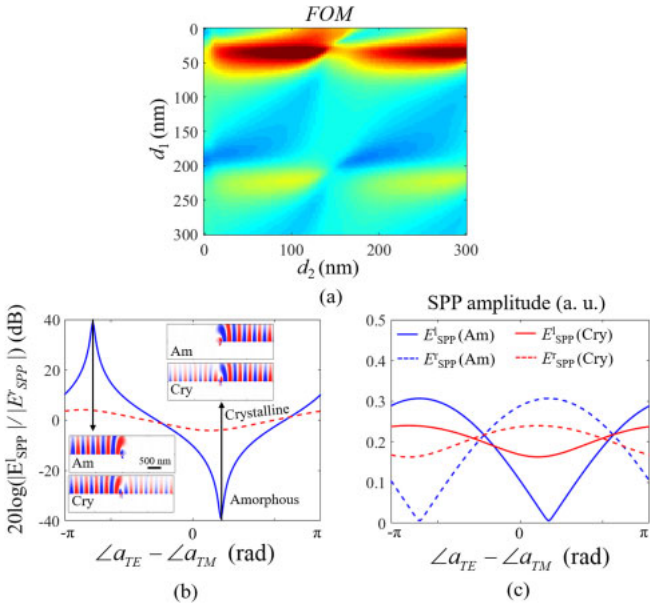

Fig. 5. (Color online) (a) Characteristic of FOM parameter of the proposed structure varying with two parameters d_1 and d_2. The FOM is defined as the ratio of TE/TM coupling ratio before and after GST crystallization. (b) Left-to-right extinction ratio characteristic of the proposed structure. Insets show the field distributions which show the greatest extinction ratio when amorphous/crystalline GST is inserted, respectively. (c) Relative amplitude of excited SPPs measured at 4 μm distanced from the slit center are plotted for various conditions — left-side, amorphous GST (blue solid); right-side, amorphous GST (blue dashed); left-side, crystalline GST (red solid); right-side, crystalline GST (red dashed); respectively.

$$\mathrm{FOM} = \frac{\text{TE/TM ratio with crystalline GST}}{\text{TE/TM ratio with amorphous GST}} = \frac{|c^{\mathrm{cry}}_{\mathrm{SPP,TE}}||c^{\mathrm{am}}_{\mathrm{SPP,TM}}|}{|c^{\mathrm{cry}}_{\mathrm{SPP,TM}}||c^{\mathrm{am}}_{\mathrm{SPP,TE}}|}. \quad (4)$$

As shown in Fig. 5(a), the highest value of FOM is observed at the position where the two appropriate GST position investigated for TE and TM polarizations [shown in Figs. 3(a) and 4(a)] are simultaneously satisfied. Figure 5(b) shows the left-to-right intensity extinction ratio of the directional SPP excitation varying with the phase difference ($\angle a_{\mathrm{TE}} - \angle a_{\mathrm{TM}}$) between two Jone's vector components. The plot clearly shows that high-performance unidirectional launching of SPPs up to 40 dB of extinction ratio can only be achieved when inserted GST film is in amorphous state, whereas very weak left-to-right extinction ratio only of 3 dB is observed for crystalline GST case. Since the proposed unidirectional launching scheme is based on the interference of SPPs having anti-symmetric and symmetric parity, the propagation direction can also be switched by tuning the phase difference between TE and TM incident component. Insets of Fig. 5(b) show the SPP field distributions for two incident polarization states which shows the greatest extinction ratio for amorphous GST case, and those for crystalline GST case at the same polarization states. In Fig. 5(c), relative amplitude of excited SPPs for on/off states are plotted for left- and right-side SPP launching to show the absolute coupling efficiency of excited SPP itself.

In conclusion, we designed the tunable plasmonic nanocavity structure for switching the directional launching of SPP operated by changing the phase state of very-thin phase change material. About 37 dB of extinction ratio for directional SPP generation is achieved, which is sufficient for classifying unidirectional on- and off-states of the proposed structure. Since various recent works consistently show that nanoscale phase change of thin-film GST is possible by both thermal and optical stimuli, we anticipate that the proposed structure shows a promising possibility for controlling near-field signals in electro-optical or all-optical scheme, which can be applied to integrated optics, near-field controlling, and active plasmonics.

Acknowledgment This work was supported by the National Research Foundation of Korea (NRF) grant funded by the Korea government Ministry of Science and ICT (Nos. 2017R1C1B2003585 and 2017R1A4A1015565).

1) W. L. Barnes, A. Dereux, and T. W. Ebbesen, Nature **424**, 824 (2003).
2) K. G. Lee and Q.-H. Park, Phys. Rev. Lett. **95**, 103902 (2005).
3) G. M. Lerman, A. Yanai, and U. Levy, Nano Lett. **9**, 2139 (2009).
4) H. Shin and S. Fan, Phys. Rev. Lett. **96**, 073907 (2006).
5) H. J. Lezec, J. A. Dionne, and H. A. Atwater, Science **316**, 430 (2007).
6) S.-Y. Lee, W. Lee, Y. Lee, J.-Y. Won, J. Kim, I.-M. Lee, and B. Lee, Laser Photonics Rev. **7**, 273 (2013).
7) C. Lu, X. Hu, H. Yang, and Q. Gong, Adv. Opt. Mater. **1**, 792 (2013).
8) S. Roh, T. Chung, and B. Lee, Sensors **11**, 1565 (2011).
9) F. Aieta, P. Genevet, M. A. Kats, N. Yu, R. Blanchard, Z. Gaburro, and F. Capasso, Nano Lett. **12**, 4932 (2012).
10) X. Ni, A. V. Kildishev, and V. M. Shalaev, Nat. Commun. **4**, 2807 (2013).
11) S.-Y. Lee, K. Kim, S.-J. Kim, H. Park, K.-Y. Kim, and B. Lee, Optica **2**, 6 (2015).
12) S.-W. Cho, J. Park, S.-Y. Lee, H. Kim, and B. Lee, Opt. Express **20**, 10083 (2012).
13) X. Yin, Z. Ye, J. Rho, Y. Wang, and X. Zhang, Science **339**, 1405 (2013).
14) J. D. Cox and F. J. Garcia de Abajo, Nat. Commun. **5**, 5725 (2014).
15) T. Low and P. Avouris, ACS Nano **8**, 1086 (2014).
16) F. J. García de Abajo, ACS Photonics **1**, 135 (2014).
17) Z. Zhang, Z. You, and D. Chu, Light: Sci. Appl. **3**, e213 (2014).
18) M. Seo, J. Kyoung, H. Park, S. Koo, H.-S. Kim, H. Bernien, B. J. Kim, J. H. Choe, Y. H. Ahn, H.-T. Kim, N. Park, Q.-H. Park, K. Ahn, and D.-S. Kim, Nano Lett. **10**, 2064 (2010).
19) P. Hosseini, C. D. Wright, and H. Bhaskaran, Nature **511**, 206 (2014).
20) Y. Chen, X. Li, X. Luo, S. A. Maier, and M. Hong, Photonics Res. **3**, 54 (2015).
21) S.-Y. Lee, Y.-H. Kim, S.-M. Cho, G. H. Kim, T.-Y. Kim, H. Ryu, H. N. Kim, H. B. Kang, C.-Y. Hwang, and C.-S. Hwang, Sci. Rep. **7**, 41152 (2017).
22) M. Wuttig, H. Bhaskaran, and T. Taubner, Nat. Photonics **11**, 465 (2017).
23) C. Ríos, M. Stegmaier, P. Hosseini, D. Wang, T. Scherer, C. D. Wright, H. Bhaskaran, and W. H. P. Pernice, Nat. Photonics **9**, 725 (2015).
24) Q. Wang, E. T. F. Rogers, B. Gholipour, C.-M. Wang, G. Yuan, J. Teng, and N. I. Zheludev, Nat. Photonics **10**, 60 (2016).
25) S.-M. Yoon, N.-Y. Lee, S.-O. Ryu, K.-J. Choi, Y.-S. Park, S.-Y. Lee, B.-G. Yu, M.-J. Kang, S.-Y. Choi, and M. Wuttig, IEEE Electron Device Lett. **27**, 445 (2006).
26) S.-Y. Lee, I.-M. Lee, J. Park, S. Oh, W. Lee, K.-Y. Kim, and B. Lee, Phys. Rev. Lett. **108**, 213907 (2012).
27) H. Kim, J. Park, and B. Lee, *Fourier Modal Method and Its Applications in Computational Nanophotonics* (CRC Press, New York, 2012) p. 66.
28) T. Chung, S.-Y. Lee, H. Yun, S.-W. Cho, Y. Lim, I.-M. Lee, and B. Lee, IEEE Access **1**, 371 (2013).
29) A. D. Rakić, A. B. Djurišić, J. M. Elazar, and M. L. Majewski, Appl. Opt. **37**, 5271 (1998).